

First-Order Correction to the Semi-Infinite Electron Gas Model of the Inversion Carriers at a Semiconductor-Insulator Interface

T. L. Li¹ and T. W. Tang²

¹*Department of Applied Physics, National Chia-Yi University,
300 Hsueh-Fu Road, Chiayi, Taiwan 600, R.O.C.*

²*Department of Electrical and Computer Engineering,
University of Massachusetts Amherst, Amherst, MA01003, USA*

(Received June 27, 2001)

The Semi-infinite Electron Gas (SEG) model in the literature is extended to explicitly include the potential energy gradient to first-order, leading to the First-Order Semi-infinite Electron Gas (FOSEG) model of this work. To study the validity of the conventional and the first-order models, the density of states and the carrier density of a triangular potential are computed by both models, and are compared with the exact solution. The field-induced state density in the conventionally forbidden bandgap can be modeled by the first-order approximation because of its explicit inclusion of the potential gradient. Comparison of the carrier density shows that, when there are enough quantum levels below the Fermi level, the first-order results match the exact solution better than the conventional model, especially at locations beyond the classical turning point associated with the Fermi energy.

PACS. 73.20.At – Surface states, band structure, electron density of states.

PACS. 73.40.Qv – Metal-insulator-semiconductor structures.

PACS. 71.10.Ca – Electron gas, Fermi gas.

I. Introduction

The Homogeneous Electron Gas (HEG) model of solid-state physics [1] has been extensively used in semiconductor physics [2, 3]. In the HEG theory, the electrons are treated as independent particles subject to a constant potential energy in an infinite space. Hence, the HEG model is more appropriate for semiconductors that are unbounded or infinite in size.

For the problem of a semiconductor-insulator interface, the HEG model has to be modified to take the unpenetrable boundary condition into account. This modification of the homogeneous electron gas model was called the Modified Local Density Approximation (MLDA) in Refs. [4, 5]. However, in more modern literature, the Local Density Approximation (LDA) usually refers to the approximation used for the exchange and the correlation energy [6-8]. To avoid confusion, the MLDA of Refs. [4, 5], which treats the quantum correction to the inversion carriers at semiconductor-insulator interface phenomenologically, is renamed as the Semi-infinite Electron Gas (SEG) model in this work, because the vanishing boundary condition at the unpenetrable interface essentially implies a semi-infinite piece of semiconductor.

In both the Homogeneous Electron Gas (HEG) model and the Semi-infinite Electron Gas (SEG) model, the potential energy of the electron is independent of the position. Thus, only

the zeroth-order position-derivative of the potential energy matters in the model. Therefore, both the HEG and the SEG can be considered as a zeroth-order theory. In the quantum-mechanical treatments of the electron gas in this zeroth-order theory, the potential energy operator commutes with the kinetic energy operator [4, 5].

For the semiconductor-insulator interface at inversion, the potential energy of the electron is position-dependent due to the band-bending caused by the electric field. Under such circumstances, the potential energy operator and the kinetic energy operator no longer commute [9], and, strictly speaking, the zeroth-order theory of the HEG and the SEG no longer holds, either.

Furthermore, it was reported in the literature that the tunneling tails of the electron wave functions into the band edge introduces a nonvanishing density of states into the conventionally forbidden bandgap with the presence of band-bending [10, 11]. This tunneling effect can not be modeled by the homogeneous and the semi-infinite electron gas models because the potential gradient is explicitly ignored in both models.

The homogeneous electron gas in infinite space had been modified to explicitly include the potential energy gradient to first-order, leading to the First-Order Homogeneous Electron Gas (FOHEG) approximation [12]. This first-order theory of the electron gas in infinite space was reported to be capable of modeling the electron tunneling effects previously ignored by the conventional zeroth-order theory. However, since the FOHEG does not take the vanishing boundary condition into account, it can not be applied to the semiconductor-insulator interface.

In this article, the SEG model is extended, by using some of the techniques developed in the FOHEG, to explicitly include the potential energy gradient to first-order for application to the inversion carriers at the semiconductor-insulator interface. This approximation is called the First-Order Semi-infinite Electron Gas (FOSEG) in this work, and is applicable to the semiconductor-insulator interface because, near the interface, the second- and higher-order derivatives of the potential energy are significantly less important than the first-order derivative.

The four approximations to the electron gas mentioned in this section are the HEG, the SEG, the FOHEG, and the FOSEG. They can be differentiated by the conditions that are taken into account by the approximations. The conditions include whether the vanishing boundary condition is considered and whether the potential gradient is explicitly accounted for. The four approximations and their employed conditions are summarized in Table I.

This article is presented in the following order. In Sec. II, the FOSEG is introduced and the analytic expressions for the density of states and the carrier density are derived. In Sec. III, the FOSEG is shown to reduce to the SEG in the literature as the electric field diminishes. In Sec. IV, to study the validity of the approximations, the density of states and the carrier density

TABLE I. Four approximations to the electron gas.

	Without potential gradient	With potential gradient
Without vanishing boundary condition	HEG	FOHEG
With vanishing boundary condition	SEG	FOSEG

of the triangular potential are computed for the FOSEG and for the SEG, and are compared with the exact solution. Finally, the article is concluded in Sec. V.

II. First-order semi-infinite electron gas model

In the theory of a homogeneous electron gas in infinite space, the electrons are treated as independent particles and individually satisfy the Schrödinger equation,

$$\hat{H}' \psi_i(\mathbf{r}) = \epsilon_i \psi_i(\mathbf{r}); \quad (1)$$

where $\hat{H} = \hat{T} + \hat{V}$ is the Hamiltonian, $\hat{T} = \frac{\hat{p}^2}{2m}$ and \hat{V} are the kinetic energy and the potential energy operators, respectively, and $\psi_i(\mathbf{r})$ and ϵ_i are, respectively, the eigenfunction and the eigenenergy. The eigenfunction is normalized by $\int \psi_i^*(\mathbf{r}) \psi_i(\mathbf{r}) d^3\mathbf{r} = 1$.

The carrier concentration can be calculated by solving Eq. (1) and summing over all of the squared moduli of wave functions weighted by the Fermi-Dirac distribution,

$$n(\mathbf{r}) = 2 \sum_i |\psi_i(\mathbf{r})|^2 f(\epsilon_i); \quad (2)$$

where

$$f(\epsilon) = \frac{1}{1 + e^{-(\epsilon - \epsilon_F)/kT}} \quad (3)$$

is the Fermi-Dirac distribution, $kT = \frac{1}{\beta}$, and ϵ_F is the Fermi level of the system. The factor of 2 in Eq. (2) is due to electron spin.

If the Non-Local Density of States (NLDS) of the electron,

$$D(\mathbf{r}; \mathbf{r}^0; \epsilon) = 2 \sum_i \pm \psi_i^*(\mathbf{r}^0) \psi_i(\mathbf{r}); \quad (4)$$

is introduced [4, 5], the carrier density can be calculated by integrating over energy the product of the Local Density of States (LDS) and the Fermi-Dirac distribution:

$$n(\mathbf{r}) = \int d\epsilon D(\mathbf{r}; \mathbf{r}; \epsilon) f(\epsilon); \quad (5)$$

where the LDS is given by

$$D(\mathbf{r}; \mathbf{r}^0) = \lim_{\epsilon \rightarrow \epsilon_F} D(\mathbf{r}; \mathbf{r}^0; \epsilon); \quad (6)$$

The NLDS in Eq. (4) can be rewritten as a \pm -operator acting on a \pm -function [13, 14],

$$D(\mathbf{r}; \mathbf{r}^0; \epsilon) = 2 \pm \psi_i \frac{1}{2} (\hat{H}_F + \hat{H}_{r^0}^\dagger) \pm(\mathbf{r}; \mathbf{r}^0); \quad (7)$$

where \hat{H}_F and $\hat{H}_{r^0}^\dagger$ are the Hamiltonian and the adjoint of the Hamiltonian operating on the \mathbf{r} - and \mathbf{r}^0 -coordinates, respectively. The completeness relation, $\int \psi_i^*(\mathbf{r}^0) \psi_i(\mathbf{r}) = \pm(\mathbf{r}; \mathbf{r}^0)$, has been utilized in deriving Eq. (7).

In order to take the boundary condition of the semiconductor-insulator interface into account, the above formulations for the homogeneous electron gas in the infinite semiconductors have to be modified. If the insulator is modeled as an unpenetrable barrier locating at the $z = 0$ plane, then the wave functions $\psi_i(\mathbf{r})$ can be expanded by a set of basis which vanishes at the interface at $z = 0$, and the NLDS for semi-infinite semiconductors can be expressed as [4, 5]

$$D(\mathbf{r}; \mathbf{r}^0; \mu) = 2 \pm \mu \int \frac{d^3 p}{(2\pi\hbar)^3} \hat{H}_F + \hat{H}_{r^0}^y \pm \mathbf{p} \cdot \mathbf{r} \pm (x_i - x^0) \pm (y_i - y^0) \pm (z + z^0) \pm \mu \mathbf{p} \cdot \mathbf{r}^0; \quad (8)$$

where $\mathbf{r} = x\mathbf{i} + y\mathbf{j} + z\mathbf{k}$ and $\mathbf{r}^0 = x^0\mathbf{i} + y^0\mathbf{j} + z^0\mathbf{k}$.

The NLDS in Eq. (8) can be decomposed into two parts,

$$D(\mathbf{r}; \mathbf{r}^0; \mu) = D_1(\mathbf{r}; \mathbf{r}^0; \mu) + D_2(\mathbf{r}; \mathbf{r}^0; \mu); \quad (9)$$

where $D_1(\mathbf{r}; \mathbf{r}^0; \mu)$ is same as the NLDS of the infinite semiconductors given by Eq. (7), and

$$D_2(\mathbf{r}; \mathbf{r}^0; \mu) = 2 \pm \mu \int \frac{d^3 p}{(2\pi\hbar)^3} \hat{H}_F + \hat{H}_{r^0}^y \pm \mathbf{p} \cdot \mathbf{r} \pm (x_i - x^0) \pm (y_i - y^0) \pm (z + z^0) \pm \mu \mathbf{p} \cdot \mathbf{r}^0; \quad (10)$$

Following the treatments in Refs. [12-16], the \pm -functions in Eqs. (7) and (10) are replaced by their integral representations. The two parts of the exact NLDS read

$$\begin{aligned} D_1(\mathbf{r}; \mathbf{r}^0; \mu) = & 2 \int \frac{d^3 p}{(2\pi\hbar)^3} \int \frac{d^3 p'}{(2\pi\hbar)^3} \frac{d!}{2^{d/2}} e^{i\mathbf{p}' \cdot \mathbf{r} + i\mathbf{p} \cdot \mathbf{r}^0} e^{i\mathbf{p} \cdot \mathbf{r}} e^{i\mathbf{p}' \cdot \mathbf{r}^0} \\ & \times \exp \left[\frac{i}{2m} (\mathbf{p}^2 + \mathbf{p}'^2) + \mathbf{p} \cdot \mathbf{r} + \mathbf{p}' \cdot \mathbf{r}^0 \right] \\ & + \frac{i}{4m} (\mathbf{p}^2 V + \mathbf{p}'^2 V^0) + \mathbf{p} \cdot \mathbf{r} + \mathbf{p}' \cdot \mathbf{r}^0 + \mathbf{p} \cdot \mathbf{r}^0 + \mathbf{p}' \cdot \mathbf{r} \\ & + \frac{i}{16m} (\mathbf{p} V)^2 + (\mathbf{p}' V^0)^2 \end{aligned} \quad (11)$$

and

$$\begin{aligned} D_2(\mathbf{r}; \mathbf{r}^0; \mu) = & 2 \int \frac{d^3 p}{(2\pi\hbar)^3} \int \frac{d^3 p'}{(2\pi\hbar)^3} \frac{d!}{2^{d/2}} e^{i\mathbf{p}' \cdot \mathbf{r} + i\mathbf{p} \cdot \mathbf{r}^0} e^{i\mathbf{p} \cdot \mathbf{r}} e^{i\mathbf{p}' \cdot \mathbf{r}^0} \\ & \times \exp \left[\frac{i}{2m} (\mathbf{p}^2 + \mathbf{p}'^2) + \mathbf{p} \cdot \mathbf{r} + \mathbf{p}' \cdot \mathbf{r}^0 \right] \\ & + \frac{i}{4m} (\mathbf{p}^2 V + \mathbf{p}'^2 V^0) + \mathbf{p} \cdot \mathbf{r} + \mathbf{p}' \cdot \mathbf{r}^0 + \mathbf{p} \cdot \mathbf{r}^0 + \mathbf{p}' \cdot \mathbf{r} \\ & + \frac{i}{16m} (\mathbf{p} V)^2 + (\mathbf{p}' V^0)^2; \end{aligned} \quad (12)$$

where μ is a parameter varying from 0 to 1, $d!$ is the infinitesimal differential of μ , and \times represents the multiplicative cascade of the infinitesimal operator following it [12, 13]. Operators

\hat{p} and \hat{p}^0 operate on the r - and r^0 -coordinates, respectively, and $V \sim V(r)$ and $V^0 \sim V(r^0)$. The Hermiticity of the Hamiltonian, $\hat{H}_{r^0}^y = \hat{H}_{r^0}$, has been used in deriving Eqs. (11) and (12). Note the notations used in Eq. (12): $r^0 = x^0 i + y^0 j + z^0 k$ and $p^0 = p_x i + p_y j + p_z k$ if $r^0 = x^0 i + y^0 j + z^0 k$ and $p = p_x i + p_y j + p_z k$.

In the first-order approximation of this work, all second and higher derivatives of the potential energy in Eqs. (11) and (12) are neglected. Since only the first-order derivative of the potential energy is retained, the approximation is called the First-Order Semi-infinite Electron Gas (FOSEG) in this article.

The approximate LDS follows from its defining equation, Eq. (6). After the integration over momentum is performed by using

$$\int_{-\infty}^{\infty} \frac{d^3 p}{(2\pi)^3} e^{i p \cdot r} = \frac{m}{2\pi i} \int_{-\infty}^{\infty} \frac{e^{-\frac{p^2}{2m}}}{i} dz; \quad (13)$$

the two parts of the LDS become

$$D_1(F; \psi) = \frac{1}{4} \frac{m}{2\pi i} \int_{-\infty}^{\infty} \frac{e^{-\frac{p^2}{2m}}}{i} dz \int_{-\infty}^{\infty} \frac{1}{i} e^{i p \cdot (r + V(r))} e^{i a^3 p \cdot z} dz; \quad (14)$$

and

$$D_2(F; \psi) = \frac{1}{4} \frac{m}{2\pi i} \int_{-\infty}^{\infty} \frac{e^{-\frac{p^2}{2m}}}{i} dz \int_{-\infty}^{\infty} \frac{1}{i} e^{i p \cdot (r + V(r))} e^{i a^3 p \cdot z} e^{i \frac{m}{2} (B + \frac{p^2}{m})^2} dz; \quad (15)$$

where $a^3 = \frac{\hbar^2 (rV)^2}{24m}$ and $B = \frac{\hbar^2 eV}{4m \omega z}$.

Observation of Eqs. (14) and (15) shows that the vanishing boundary condition at $z = 0$ is not fulfilled unless $B = 0$. Note that, in Eq. (15), B is of first-order in the power of the potential gradient; whereas, a^3 is of second-order. In the inversion layer of semiconductor-insulator interface, the potential gradient is large. Hence, the first-order term (the B -term) is less important than the second-order term (the a^3 -term), and is ignored in the subsequent computation to ensure that the boundary condition at $z = 0$ is satisfied.

Therefore, the LDS is obtained by combining D_1 and D_2 ,

$$D(F; \psi) = \frac{1}{4} \frac{m}{2\pi i} \int_{-\infty}^{\infty} \frac{e^{-\frac{p^2}{2m}}}{i} dz \int_{-\infty}^{\infty} \frac{1}{i} e^{i p \cdot (r + V(r))} e^{i a^3 p \cdot z} (1 + e^{i \frac{c}{r}}) dz; \quad (16)$$

$$= i \frac{1}{4} \frac{m}{2\pi i} \int_{-\infty}^{\infty} \frac{e^{-\frac{p^2}{2m}}}{i} dz \sum_{n=1}^{\infty} \frac{(ic)^n}{n!} \int_{-\infty}^{\infty} \frac{1}{i^{n+\frac{3}{2}}} e^{i p \cdot (r + V(r))} e^{i a^3 p \cdot z} dz; \quad (17)$$

$$= i \frac{1}{4} \frac{m}{2\pi i} \int_{-\infty}^{\infty} \frac{e^{-\frac{p^2}{2m}}}{i} dz \sum_{n=1}^{\infty} \frac{(ic)^n}{n!} \int_{-\infty}^{\infty} dt Ai(t) \frac{1}{i^{n+\frac{3}{2}}} \int_{-\infty}^{\infty} \frac{1}{i^{n+\frac{3}{2}}} e^{i p \cdot (r + V + bt)} dz; \quad (18)$$

$$= i \frac{1}{2} \frac{m}{2\pi i} \int_{-\infty}^{\infty} \frac{e^{-\frac{p^2}{2m}}}{i} dz \int_{-\infty}^{\infty} dt Ai(t) (1+t)^{\frac{1}{2}} \sum_{n=1}^{\infty} \frac{[icb(1+t)]^n}{n! \Gamma(n + \frac{3}{2})}; \quad (19)$$

$$= \frac{4}{\pi^{1/4}} \frac{m}{2^{1/4} \sim 2} \int_{-1}^{\infty} dt \text{Ai}(t) (\eta + t)^{1/2} j_0 \left(\frac{h}{2} \sqrt{c} (\eta + t) \right); \quad (20)$$

where $c = \frac{2mz^2}{\sim 2}$, $b = \frac{b}{3a}$, $\eta = \frac{\eta_i V}{b}$, and $\sqrt{c} = z^2 \left(\frac{m j r V j}{\sim 2} \right)^{1/3}$. Equation (17) follows by the series expansion of $e^{i \eta t}$. Formulae [17-19]

$$e^{i \eta t} = \int_{-1}^{\infty} dt \text{Ai}(t) e^{i \eta t}; \quad (21)$$

$$\frac{1}{2^{1/4} \Gamma(n + \frac{3}{2})} \int_{-1}^{\infty} dt t^n e^{i \eta t} = \frac{1}{\Gamma(n + \frac{3}{2})} \mu^{(n)}; \quad (22)$$

for $n = 0; 1; 2; \dots$, and [20, 21]

$$\sum_{n=0}^{\infty} \frac{(x^2)^n}{n! \Gamma(n + \frac{3}{2})} = j_0(2x) \quad (23)$$

are utilized to obtain Eqs. (18), (19), and (20), respectively. Ai , Γ , μ , and j_0 are the Airy function, the Gamma function, the unit step function, and the spherical Bessel function of the first kind, respectively [22]. Pachhammer's notation [22], $(z)_n = (z)(z + 1)(z + 2) \dots (z + n - 1)$ is used in Eq. (23) with $z = \frac{3}{2}$.

Once the LDS is obtained, the carrier density follows directly from Eq. (5),

$$n(F) = \frac{4}{\pi^{1/4}} \frac{mb}{2^{1/4} \sim 2} \int_{-1}^{\infty} dt \text{Ai}(t) (\eta + t)^{1/2} j_0 \left(\frac{h}{2} \sqrt{c} (\eta + t) \right) f(\eta); \quad (24)$$

where $f(\eta) = 1/[1 + e^{-\eta}]$ is the Fermi-Dirac distribution in normalized notations: $\eta = \frac{b}{kT}$, $\eta = \frac{\eta_i V}{b}$, and $\eta_F = \frac{\eta_i V}{b}$. Note that $f(\eta) = f(\eta - \eta_F)$. Also note that the first integral over t in Eq. (24) comes from the LDS.

III. Relations to semi-infinite electron gas

In this section, it will be shown that the First-Order Semi-infinite Electron Gas (FOSEG) of this work reduces to the Semi-infinite Electron Gas (SEG) in the literature, as the potential gradient gradually diminishes. Specifically, it will be shown that the LDS in Eq. (20) and the carrier density in Eq. (24) both approach the flat-band equations of the SEG as the potential energy gradient approaches zero.

The analysis of the limiting behavior of LDS in Eq. (20) is divided into two cases, depending on the sign of $(\eta_i V)$. First, suppose that $(\eta_i V) > 0$. As $j r V j \rightarrow 0$, $b \rightarrow 0$, then $\eta \rightarrow 1$ and $b \eta = \eta_i V$. Equation (20) is rewritten as

$$D(F; \eta) = \frac{4}{\pi^{1/4}} \frac{m}{2^{1/4} \sim 2} \int_{-1}^{\infty} dt \text{Ai}(t) (\eta_i V + t)^{1/2} j_0 \left(\frac{h}{2} \sqrt{c} (\eta_i V + t) \right) \\ = \frac{m}{\sim 2} \frac{2m}{\sim 2} (\eta_i V) j_0 \left(\frac{2m}{\sim 2} (\eta_i V) \right); \quad (25)$$

where the integral $\int_0^{\infty} A_i(t) dt = 1$ has been used in Eq. (25) [22].

Second, suppose that $(\mu_i - V) < 0$. As $|j_r - V_j| \rightarrow 0$, $b \rightarrow 0$, then $\mu_i \rightarrow \mu_i - 1$. The integration interval diminishes. Hence, $D(F; \mu) \rightarrow 0$.

Sequently, the LDS in Eq. (24) becomes

$$D(F; \mu) = \frac{m}{\sqrt{4\pi} \cdot 2} \int_0^{\infty} \frac{2m}{\sqrt{2}} (\mu_i - V) \cdot \frac{1}{1 + j_0} \cdot \frac{\tilde{A}}{2z} \cdot \frac{1}{\sqrt{2}} (\mu_i - V) \cdot \mu(\mu_i - V); \quad (26)$$

as $|j_r - V_j| \rightarrow 0$, which is indeed same as the flat-band results obtained by the semi-infinite electron gas in Ref. [4].

The carrier density at the low-gradient limit follows from Eq. (5), as $|j_r - V_j| \rightarrow 0$,

$$n(F) = \frac{2N_c}{\sqrt{4\pi}} \int_0^{\infty} d\mu \gg \frac{1}{2} \int_0^{\infty} \frac{\mu}{L} \gg \frac{1}{2} \frac{1}{1 + e^{\mu_i - \mu}}; \quad (27)$$

where $N_c = 2 \frac{1}{\sqrt{4\pi}} \frac{m k T}{2m k T} \frac{c^3}{2}$, $L = \frac{1}{2m k T}$, and $\mu_i = \mu_i - V$. Equation (27) is the carrier density of the semi-infinite electron gas reported in Ref. [4].

Therefore, the LDS and the carrier density obtained by the FOSEG of this work indeed reduce to the flat-band equations of the SEG as the potential energy gradient diminishes. This reduction will be confirmed numerically in the next section.

IV. Result and discussion

In contrast to the Semi-infinite Electron Gas (SEG) theory, the First-Order Semi-infinite Electron Gas (FOSEG) theory of this work explicitly takes the first-order gradient of the potential energy into account.

In order to study the validity of both approximate methods, the Local Density of States (LDS or, simply, DOS) and the carrier density are calculated by the FOSEG and by the SEG, and are compared with the exact solution for the triangular potential

$$V(F) = eFz \quad \text{if } z > 0 \\ 1 \quad \text{if } z < 0 \quad (28)$$

where e is the magnitude of the electron charge, F is the electric field, and z is the normal distance to the interface.

The exact DOS and the exact carrier concentration of the triangular potential are given in Ref. [23] by

$$D(F; \mu) = \frac{m}{\sqrt{4\pi} \cdot 2} \sum_{n=1}^{\infty} j_{\tilde{A}_n(z)}^2 \mu(\mu_i - E_n); \quad (29)$$

and

$$n(F) = \frac{m k T}{\sqrt{4\pi} \cdot 2} \sum_{n=1}^{\infty} j_{\tilde{A}_n(z)}^2 \ln \frac{h}{1 + e^{-(E_n - \mu_i - F)}}; \quad (30)$$

respectively, where the eigenenergy and the eigenfunction of the one-dimensional potential are given by

$$E_n = \frac{(\sim eF)^{2/3}}{(2m)^{1/3}} j S_n; \quad (31)$$

and

$$\tilde{A}_n(z) = \frac{\mu}{\sim^2} \frac{2meF}{\sim^2} \eta^{1/6} \frac{1}{jAi'(S_n)} Ai \left(\frac{\tilde{A}}{\mu} \frac{2meF}{\sim^2} \eta^{1/3} \mu z \right) \frac{E_n}{eF} \eta^{1/6}; \quad (32)$$

respectively, where S_n is the n -th zero of the Airy function, namely, $Ai(S_n) = 0$, for $n = 1; 2; \dots$. Note that S_n is negative.

In all of the calculations of this work, the electron mass is taken to be the effective-mass of the silicon electron, $m = 1.18 m_0$, where m_0 is the electron rest mass, and the temperature is taken to be at 300 K.

The DOS of the triangular potential obtained from the exact solution in Eq. (29), from the FOSEG in Eq. (20), and from the SEG in Eq. (26) are plotted in solid, dashed, and dotted lines, respectively, for the electric field of 1 MV/cm in Figs. 1 and 2. The DOS at other electric fields is qualitatively similar and is, thus, not shown.

In Fig. 1, the DOS is plotted as a function of energy at location $z = 5$ nm on a logarithmic scale. The DOS obtained by the conventional SEG vanishes as the energy ϵ is below the conduction band edge at $V(z = 5 \text{ nm}) = 0.5$ eV. However, the exact solution exhibits nonvanishing DOS below the band edge.

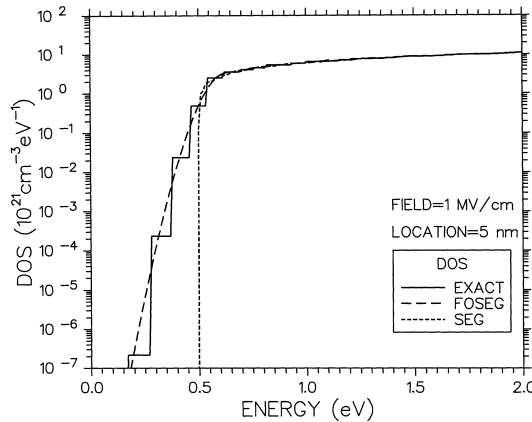


FIG. 1. The DOS of a triangular barrier with the electric field of 1 MV/cm is plotted versus energy at location $z = 5$ nm. The DOS's obtained by the exact solution, the FOSEG, and the SEG are plotted in solid, dashed, and dotted lines, respectively.

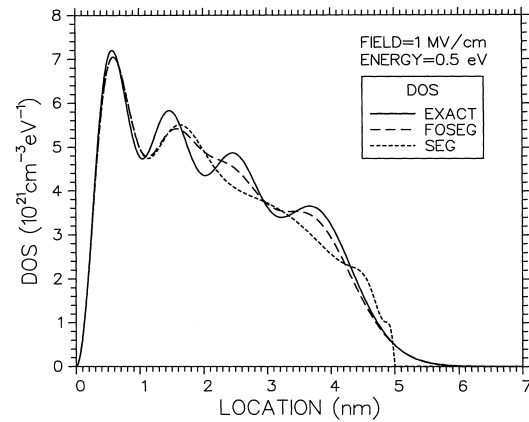


FIG. 2. The DOS of a triangular barrier with the electric field of 1 MV/cm is plotted versus location at energy $\epsilon = 0.5$ eV. The DOS's obtained by the exact solution, the FOSEG, and the SEG are plotted in solid, dashed, and dotted lines, respectively.

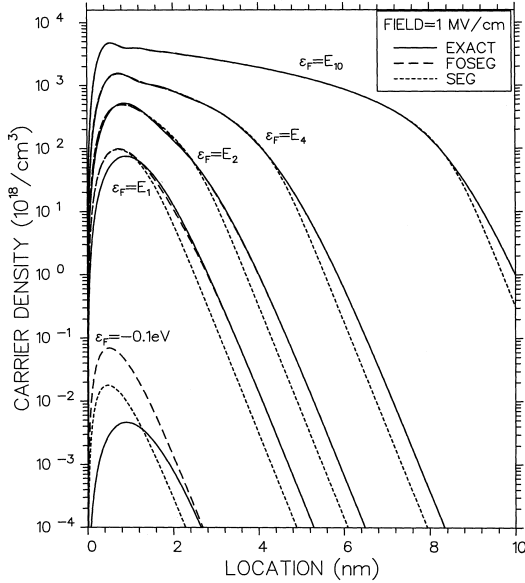


FIG. 3. The carrier density of a triangular barrier with the electric field of 1 MV/cm is plotted for Fermi levels $\epsilon_F = i$ 100, 160.41 (E_1), 280.45 (E_2), 465.60 (E_4), and 880.11 (E_{10}) meV. The carrier densities obtained by the exact solution, the FOSEG, and the SEG are plotted in solid, dashed, and dotted lines, respectively.

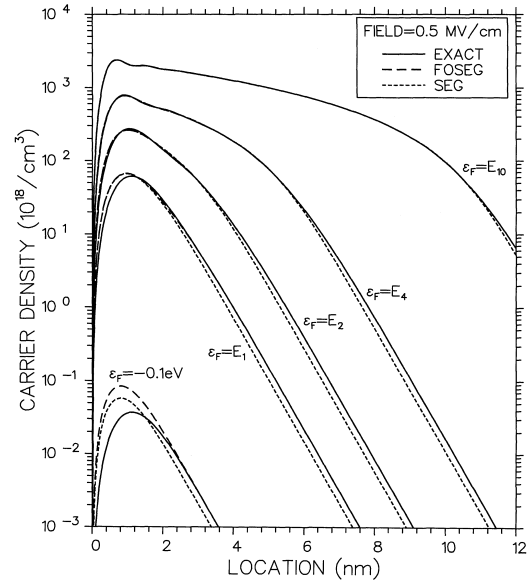


FIG. 4. The carrier density of a triangular barrier with the electric field of 0.5 MV/cm is plotted for Fermi levels $\epsilon_F = i$ 100, 101.05 (E_1), 176.68 (E_2), 293.31 (E_4), and 554.44 (E_{10}) meV. The carrier densities obtained by the exact solution, the FOSEG, and the SEG are plotted in solid, dashed, and dotted lines, respectively.

In Fig. 2, the DOS is plotted as a function of location for energy $\epsilon = 0.5$ eV in linear scale. The DOS predicted by the conventional SEG vanishes beyond the classical turning point at $z = 5$ nm. But, the exact results exhibit a nonvanishing tail beyond the classical turning point.

In Fig. 2, the DOS is plotted as a function of location for energy $\epsilon = 0.5$ eV in linear scale. The DOS predicted by the conventional SEG vanishes beyond the classical turning point at $z = 5$ nm. But, the exact results exhibit a nonvanishing tail beyond the classical turning point.

The nonvanishing DOS below the band edge and beyond the classical turning point illustrated in Figs. 1 and 2, respectively, is due to the quantum-mechanical tunneling of wave functions, in the presence of the electric field, into the semiconductor beyond the turning point. The tunneling effectively lowers the conduction band edge, and consequently reduces the bandgap [10, 11].

The conventional SEG theory can not model this tunneling effect because of the explicit negligence of the potential gradient in its formalism. On the contrary, the FOSEG theory of this work accounts for the potential gradient to the first-order, and is more capable of modeling the tunneling effects than the SEG theory.

The carrier densities as functions of the location are plotted in Figs. 3, 4, and 5 for electric field $F = 1, 0.5$ and 0.1 MV/cm, respectively. In each figure, the carrier densities for Fermi levels

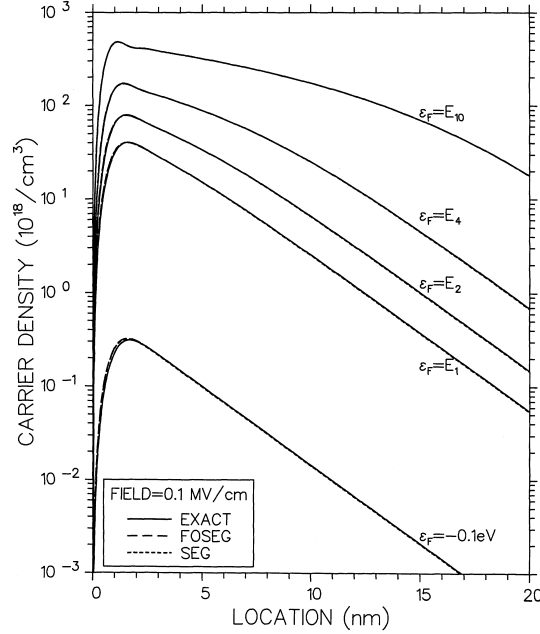


FIG. 1. The carrier density of a triangular barrier with the electric field of 0.1 MV/cm is plotted for Fermi levels $\epsilon_F = i$ 100, 34.56 (E_1), 60.42 (E_2), 100.31 (E_4), and 189.62 (E_{10}) meV. The carrier densities obtained by the exact solution, the FOSEG, and the SEG are plotted in solid, dashed, and dotted lines, respectively.

TABLE II. Eigen energies of a triangular barrier under electric field F .

Field (MV/cm)	E_1 (meV)	E_2 (meV)	E_4 (meV)	E_{10} (meV)
$F = 1$	160.41	280.45	465.60	880.11
$F = 0.5$	101.05	176.68	293.31	554.44
$F = 0.1$	34.56	60.42	100.31	189.62

at i 0.1 eV, the first (E_1), the second (E_2), the fourth (E_4), and the tenth (E_{10}) eigenenergies of the triangular barrier are depicted. The eigenenergies of the above-mentioned eigenlevels are different for the triangular barrier under different electric fields, and are tabulated in Table II.

The inversion carriers at the interface under a strong electric field of 1 MV/cm is plotted in Fig. 3. Three features are observed in this carrier density plot.

First, at low Fermi energy such as $\epsilon_F = i$ 0.1 eV and E_1 , both the FOSEG and SEG greatly deviate from the exact carrier density. (Although the FOSEG agrees better with the exact carrier density at the tail than the SEG, this is not of much significance because the peak concentration is

off by almost an order of magnitude.) It is found that, at an electric field of 1 MV/cm, there must be at least four quantum levels below the Fermi level for the FOSEG results to be sufficiently close to the exact solution. At Fermi energy $\mu_F = E_4$ and E_{10} , the FOSEG lines are indistinguishable from the exact lines in the figure.

Second, The FOSEG results with successively higher Fermi energy ($\mu_F = \{ 0.1 \text{ eV}, E_1, E_2, E_4, \text{ and } E_{10} \}$) show that systems with more quantum levels below the Fermi energy better approach the exact solution, demonstrating the statistical nature of the approximation.

Third, at the classical turning point associated with the Fermi energy (given by the location $z_F = \mu_F / (eF)$), the carrier density obtained by the conventional SEG starts to deviate more significantly from the exact solution, but the FOSEG well matches the exact results. This is due to the fact that the tunneling of the wave functions beyond the classical turning point is included in the formalism of the FOSEG as illustrated in Figs. 1 and 2.

Figure 4 shows the carrier density at the electric field of 0.5 MV/cm. The three features observed in Fig. 3 and stated in the above paragraphs for the field of 1 MV/cm also hold qualitatively for this field.

The carrier density at a lower electric field of 0.1 MV/cm is shown in Fig. 5. The curves for the exact solution, the FOSEG, and the SEG are almost indistinguishable. This is a numerical verification of the SEG being the low-field limit of the FOSEG as indicated by the analysis in Sec. III.

From Figs. 3, 4, and 5, it found that the system must have a large enough number of quantum levels below the Fermi level for the FOSEG to sufficiently approach the exact solution, and that the number of quantum levels below the Fermi energy increases with the electric field (for example, four and two levels for $F = 1$ and 0.1 MV/cm, respectively). Hence, it is claimed in this article that, under all practical strengths of electric field, the FOSEG is a good approximation to the exact solution if there are at least four quantum levels below the Fermi level, a condition termed the “four-level condition” in this work.

V. Conclusions

The Semi-infinite Electron Gas (SEG) in the literature is extended to include the first-order derivative of the potential energy, resulting in the First-Order Semi-infinite Electron Gas (FOSEG) of this work. The FOSEG is applicable to the inversion carriers at semiconductor-insulator interface.

With the FOSEG, the density of states and the carrier density are given by analytic expressions in Eqs. (20) and (24), respectively. These equations reduce to the SEG results reported in the literature as the electric field gradually diminishes.

To study the validity of the approximations, the density of states and the carrier density of a triangular potential are computed by the FOSEG and the SEG, and are compared with the exact solution.

In contrast to the SEG, the FOSEG explicitly includes the potential energy gradient in its formalism, and is capable of accounting for the tunneling of electron wave functions beyond the classical turning point. Hence, the nonvanishing density of states below the band edge at the presence of the electric field can be modeled by the FOSEG of this work, but was completely ignored by the SEG.

It is found that the FOSEG results better match the exact solution for systems with more

quantum levels below the Fermi level, demonstrating the statistical nature of the approximation. Moreover, at location beyond the classical turning point associated with the Fermi energy, the carrier density obtained by the FOSEG matches the exact solution better than the SEG because of its explicit inclusion of the potential energy gradient in the formulations of the FOSEG.

Acknowledgments

T. L. Li acknowledges the support of the National Science Council, Taiwan, by Grant NSC90-2215-E-415-001. T. W. Tang acknowledges the support from the National Science Foundation, U. S., under NSF Grant ECS-9710463 and a grant from the National Science Council through the National Center of High-performance Computing in Hsinchu, Taiwan.

References

*Corresponding author: T. L. Li (quantum@mail.ncyu.edu.tw).

- [1] N. W. Ashcroft and N. D. Mermin, *Solid state physics* (W. B. Saunders Company, Philadelphia, 1976).
- [2] R. F. Pierret, *Semiconductor device fundamentals* (Addison-Wesley Publishing Company, Reading, Massachusetts, 1996).
- [3] S. M. Sze, *Physics of semiconductor devices*, 2nd ed. (John Wiley & Sons, New York, 1981).
- [4] G. Paasch and H. Ubensee, *Phys. Stat. Sol. (b)* **113**, 165 (1982).
- [5] G. Paasch and H. Ubensee, *Phys. Stat. Sol. (b)* **118**, 255 (1983).
- [6] R. M. Dreizler and E. K. U. Gross, *Density functional theory – an approach to the quantum many-body problem* (Springer-Verlag, Berlin, 1990).
- [7] X. Gonze, P. Ghosez, and R. W. Godby, *Phys. Rev. Lett.* **74**, 4035 (1995).
- [8] I. I. Mazin and D. J. Singh, *Phys. Rev. B* **57**, 6879 (1998).
- [9] J. J. Sakurai, *Modern quantum mechanics* (Benjamin/Cummings Publishing, California, 1985).
- [10] J. H. Davies and J. W. Wilkins, *Phys. Rev. B* **38**, 1667 (1988).
- [11] J. R. Lowney and H. S. Bennett, *J. Appl. Phys.* **65**, 4823 (1989).
- [12] T. L. Li, *Chin. J. Phys.* **39**, 453 (2001).
- [13] V. W. Macke and P. Rennert, *Ann. Phys.* **7**, 84 (1963).
- [14] V. W. Macke and P. Rennert, *Ann. Phys.* **7**, 32 (1963).
- [15] L. C. R. Alfred, *Phys. Rev.* **121**, 1275 (1961).
- [16] L. C. R. Alfred, *Phys. Rev.* **125**, 214 (1962).
- [17] F. Oberhettinger, *Tables of Fourier transforms and Fourier transforms of distributions* (Springer-Verlag, Berlin, 1990).
- [18] H. Bateman, *Higher transcendental functions* (MacGraw-Hill Book Company, New York, 1953), Vol. I, compiled by the staff of the Bateman Manuscript Project.
- [19] R. V. Churchill, J. W. Brown, and R. F. Verhey, *Complex variables and applications*, 3rd ed. (McGraw-Hill, New York, 1974).
- [20] E. R. Hansen, *A table of series and products* (Prentice-Hall, Englewood Cliffs, 1975).
- [21] I. S. Gradshteyn and I. M. Ryzhik, *Tables of integrals, series and products*, corrected and enlarged ed. (Academic Press, New York, 1980).
- [22] M. Abramowitz and I. E. Stegun, *Handbook of mathematical functions with formulas, graphs, and mathematical tables* (National Bureau of Standards, USA, 1972).
- [23] A. P. Gnadinger and H. E. Talley, *Solid-State Electron.* **13**, 1301 (1970).